A Density Functional Theory Study of the Hydrates of $NH_3 \cdot H_2SO_4$ and Its Implications for the Formation of New Atmospheric Particles

James C. Ianni* and Alan R. Bandy

Department of Chemistry, Drexel University, Philadelphia, Pennsylvania 19104

Received: September 3, 1998; In Final Form: December 4, 1998

Density functional molecular orbital theory was used at the B3LYP/ 6-311++G(2d,2p)//B3LYP/6-311++G-(2d,2p) level of theory to study the hydrates of $NH_3 \cdot H_2SO_4 \cdot nH_2O$ for $n = 0-5$ and $NH_3 \cdot (H_2SO_4)_2 \cdot H_2O$. Neutrals of the first four $NH_3 \cdot H_2SO_4 \cdot nH_2O$ clusters ($n = 0-4$) spontaneously formed and were determined to be hydrogen-bonded molecular complexes of H_2SO_4, H_2O, and NH_3. Double ions (clusters containing a NH_4^+ cation and a HSO_4^- anion) spontaneously formed in clusters of $NH_3 \cdot H_2SO_4 \cdot nH_2O$ where $n = 1-5$. The energetics of the hydration and isomerization reactions also were calculated. Double ions are not energetically favorable until $NH_3 \cdot H_2SO_4 \cdot 4H_2O$. The free energy of formation from free NH_3 and $H_2SO_4 \cdot nH_2O$ had a maximum at $n = 3$ at room temperature with $\Delta G \approx -3$ kcal/mol. $NH_3 \cdot (H_2SO_4)_2 \cdot H_2O$ was studied to see if NH_3 can initiate new atmospheric particle growth. It has been shown that NH_3 has no role in the initialization of new atmospheric particles.

Introduction

The interest in tropospheric and stratospheric aerosols has risen in past years. This is primarily due to the fact that aerosols in the troposphere and stratosphere are altering the earth's climate by scattering radiation directly[1,2] or indirectly by changing the reflectivity of clouds.[3,4] They have also been involved in indirectly depleting the Antarctic stratospheric ozone layer by converting relatively inert chlorine species HOCl, $ClONO_2$, and HCl to photochemically reactive species such as Cl_2[5] which are well-known ozone-destroying species.[6] They can also change the chemistry of the stratosphere in general.[7] The study of the formation and evolution of these aerosols can thus be considered of utmost importance. Previously, we have shown that these aerosols can grow by a dendrimer-like sprouting mechanism[8] through attachment of $-H_2SO_4 \cdot 2H_2O-$ monomers. Unfortunately, the mechanism cannot initialize this growing process due to a too large decrease in entropy. One possible way around this obstacle is that there is a third (or more) species present which "helps" the system stabilize the initial starting clusters of $(H_2SO_4)_2 \cdot 2H_2O$ and/or increase the concentration of $X \cdot H_2SO_4 \cdot nH_2O$ ($n = 2, 4, 6$) where X is some stabilizing species. One possible species is NH_3. Recently, there has been considerable interest in this species for its possible role in new atmospheric particle formation.[9−11]

A number of studies demonstrate that ammonium sulfate and/or ammonium bisulfate are possible important species responsible for new atmospheric particle formation. One of the first identifications of ammonium sulfate in atmospheric aerosols was accomplished by Friend et al.[12] employing electron diffraction methods. Later, other researchers[13] also utilized electron diffraction to identify crystals of ammonium bisulfate. In addition, Cunningham et al.[14] employed a Raman spectroscopic method to identify ammonium sulfate in their stratospheric aerosols. Although Hayes et al.[15] raised questions about those electron diffraction measurements that detected the presence of ammonium bisulfate in stratospheric aerosols as being possibly contaminated by the NH_3 that is present at about 100 ppb in normal laboratory environments. He found that samples could quickly become contaminated with ammonia if left exposed to the laboratory environment. Today, it is commonly accepted that many early stratospheric aerosol measurements were contaminated with tropospheric ammonia (with a typical scatter of 20%[16]) after they were sampled. The question of the importance of ammonia's involvement in rapid aerosol formation has still not been resolved.[17]

In addition, some recent studies show that ammonia's participation in rapid aerosol formation could be very important due to their observations and comparison with homogeneous nucleation theory.[9,10,18] The measurement of particles in the ranges 3−500 nm by Weber et al.[10] have shown large productions of particles. A particle production rate was calculated by Weber et al.[10] using homogeneous nucleation theory[19] and assuming a binary system of only $H_2SO_4-H_2O$. The calculated production rate underestimates the experimental production rate by orders of magnitude. Weber et al. state that a ternary system of $NH_3-H_2SO_4-H_2O$ can possibly explain this low production rate, but there is contradictory evidence as shown by Nolan.[20] Nolan's aerosol formation experiments have shown no correlation in the measurement of new particles over 3 orders of magnitude of ammonia concentration in a system of $SO_2-H_2O-NH_3-$oxidizer. Clearly, there is confusion as to whether NH_3 is an important atmospheric species responsible for new atmospheric particle formation. This study will address that question.

Computational Details

To gain insight into this problem we used high-level density functional molecular orbital methods to investigate the energetics and molecular structures of $NH_3 \cdot H_2SO_4 \cdot nH_2O$ clusters from $n = 0$ to 5 and the structure and energetics of $NH_3 \cdot (H_2SO_4)_2 \cdot H_2O$. These results were obtained with density functional methods at the B3LYP/6-311++G(2d,2p)//B3LYP/6-311++G-(2d,2p) level of theory[21] as implemented in the Gaussian 94 program.[22] We chose this level of theory because it is known to give good results for hydrogen-bonded systems.[23−27]

10.1021/jp983608r CCC: $18.00
Published on Web 04/01/1999

Free energies were calculated as follows:

$$\Delta G = \Delta H - T\Delta S$$
$$\Delta H = \Delta E + \Delta(\mathrm{PV}) = \Delta E + \Delta nRT$$
$$\Delta E = \Delta E_e^{\,0} + \Delta E_{\mathrm{Thermal}}$$
$$\Delta E_{\mathrm{Thermal}} = \Delta\mathrm{ZPVE} + \Delta E_{\mathrm{vib}} + \Delta E_{\mathrm{rot}} + \Delta E_{\mathrm{tran}}$$

where ΔG is the free energy change of the reaction, ΔH is the enthalpy change, Δn is the change in moles of the reaction, R is the gas constant, ΔS is the entropy change, ΔE is the energy difference, $\Delta E_e^{\,0}$ is the difference in electronic energy at 0 K, $\Delta E_{\mathrm{Thermal}}$ contains the difference in the zero-point vibrational energy at 0 K and ΔE_{vib}, ΔE_{rot}, and ΔE_{tran} are the differences in vibrational, rotational, and translational energies, respectively, at temperature T and 1 atm. Table 1 contains all the values required for the above free energy calculation. None of the vibrational frequencies were scaled due to the fact that the scaling factor for B3LYP is close to unity.[28] In addition, no basis set superpositional errors (BSSE) were computed since it has been demonstrated that B3LYP with very large basis sets (such as the one used in this study) almost have a negligible BSSE error.[27]

We have tried to find the global minimums to the structures $NH_3{\cdot}H_2SO_4{\cdot}nH_2O$ ($n = 0$ to 5) by starting at various geometries that maximize the hydrogen bond interaction between H_2SO_4, NH_3, and H_2O. In addition, many double-ion pairs of $NH_4^+{\cdot}HSO_4^-{\cdot}nH_2O$ ($n = 0$ to 5) were investigated by similar methods but by starting with NH_4^+ and HSO_4^-. Maximizing the amount of $-$SOH....OH_2 and $-$SO....H_2O hydrogen bonds in the $H_2SO_4-H_2O$ system has been shown[31] to be a good method to obtain structures that are excellent candidates for global minimums. This method should also work for the $NH_3-H_2SO_4-H_2O$ system by also maximizing the amount of $-$SOH....NH_3 hydrogen bonds as well as the $-$SOH....OH_2 and $-$SO....H_2O hydrogen bonds. All geometries were converged to a root mean square (RMS) and maximum force of at least 3×10^{-4} and 4.5×10^{-4} hartrees/bohr, respectively. In most cases, RMS and maximum forces were much lower. RMS and maximum displacements were converged to 1.2×10^{-3} and 2×10^{-3} Å, respectively, or better. The energy in the SCF step was set to converge at 1×10^{-9} hartrees. The minima were verified with a frequency analysis. Those structures that had one or more negative frequencies were excluded from this study.

Results and Discussion

Optimized Geometries. For an accurate description of the hydrogen bonds, which are essentially holding these structures together as well as determining their geometry, we will be using hydrogen bond descriptors (HBD) in our discussion. The HBD will be enclosed in parentheses and contain three values: (acceptor length, donor length, supplement angle). Acceptor length will show the intermolecular length (in angstroms) of the acceptor oxygen to hydrogen distance (OH$\cdots$O). Donor length will show the intramolecular distance (in angstroms) between the donor's hydrogen and oxygen (O$-$H). The supplement angle value will show the deviation from linearity between the three atoms: $180° - \angle$O$-$H$\cdots$O. Neutrals in this paper will be defined as those molecules that do not contain separated ions. Structures containing an ion and a separated contraion will be known as double ions. A shorthand notation is sometimes used for representing neutrals with the formula $NH_3{\cdot}H_2SO_4{\cdot}nH_2O$ with SN***n*** where ***n*** = 0$-$5 and double ions with the formula $NH_4^+{\cdot}HSO_4^-{\cdot}nH_2O$ with SN***n***D where ***n*** = 1$-$5. Additional less stable conformers are denoted by the roman numeral II.

TABLE 1: DFT Results for Individual Molecules[a]

	temp (K)	E_{Elec}	ZPVE	E_{Thermal}	S
		Neutrals			
NH_3	298	−56.586193	21.5	23.3	48.1
	273			23.2	47.4
	248			23.0	46.6
	223			22.9	45.8
	198			22.7	44.8
	173			22.6	43.7
$NH_3{\cdot}H_2SO_4$	298	−756.997996	47.6	52.8	89.8
	273			52.2	87.3
	248			51.5	84.7
	223			50.9	81.9
	198			50.4	79.0
	173			49.9	76.0
$NH_3{\cdot}H_2SO_4{\cdot}H_2O$	298	−833.476932	63.5	70.4	104.2
	273			69.5	100.9
	248			68.6	97.5
	223			67.8	93.9
	198			67.1	90.1
	173			66.4	86.1
$NH_3{\cdot}H_2SO_4{\cdot}2H_2O$	298	−909.956007	79.3	87.8	119.1
	273			86.7	115.1
	248			85.7	110.9
	223			84.7	106.5
	198			83.8	101.8
	173			82.9	96.9
$NH_3{\cdot}H_2SO_4{\cdot}3H_2O$	298	−986.434361	94.2	104.4	131.7
	273			103.1	126.9
	248			101.8	121.9
	223			100.6	116.7
	198			99.5	111.1
	173			98.5	105.2
$NH_3{\cdot}H_2SO_4{\cdot}3H_2O$-II	298	−986.433376	95.0	105.2	133.2
$NH_3{\cdot}H_2SO_4{\cdot}4H_2O$	298	−1062.910696	109.8	121.8	146.8
	273			120.2	141.2
	248			118.8	135.4
	223			117.4	129.2
	198			116.0	122.8
	173			114.8	115.9
$NH_3{\cdot}H_2SO_4{\cdot}4H_2O$-II	298	−1062.910995	110.3	122.2	144.0
		Double Ions			
$NH_4^+{\cdot}H_2O{\cdot}HSO_4^-$	298	−833.477443	64.0	70.6	101.8
$NH_4^+{\cdot}2H_2O{\cdot}HSO_4^-$	298	−909.960358	80.6	88.8	113.1
$NH_4^+{\cdot}2H_2O{\cdot}HSO_4^-$ -II	298	−909.955902	80.0	88.1	115.4
$NH_4^+{\cdot}3H_2O{\cdot}HSO_4^-$	298	−986.437329	96.3	106.3	127.6
$NH_4^+{\cdot}3H_2O{\cdot}HSO_4^-$ -II	298	−986.437879	96.8	106.6	125.4
$NH_4^+{\cdot}4H_2O{\cdot}HSO_4^-$	298	−1062.920249	112.4	123.8	139.2
	273			122.3	141.2
	248			120.9	128.0
	223			119.5	122.0
	198			118.2	115.7
	173			117.1	109.1
$NH_4^+{\cdot}4H_2O{\cdot}HSO_4^-$ -II	298	−1062.916861	112.3	123.8	142.3
$NH_4^+{\cdot}5H_2O{\cdot}HSO_4^-$	298	−1139.397276	128.2	141.4	154.7
	273			139.7	148.4
	248			138.0	141.9
	223			136.5	135.0
	198			135.0	127.8
	173			133.6	120.2
$NH_4^+{\cdot}5H_2O{\cdot}HSO_4^-$ -II	298	−1139.397394	128.3	141.4	154.0
$NH_4^+{\cdot}H_2O{\cdot}H_2SO_4{\cdot}HSO4^-$	298	−1533.894625	90.6	100.7	128.9

[a] E_{Thermal} and ZPVE are in kcal/nol, S is in cal/(mol K), and E_{elec} is in hartree/mol.

Neutrals. Structures for $NH_3{\cdot}H_2SO_4{\cdot}nH_2O$ ($n = 0-5$) are shown in Figure 1. Figure 2 shows a general trend of the HBD's of each neutral. Column A of Figure 2 shows the donor's intermolecular hydrogen bond distance with increasing hydrate size, column B of Figure 2 shows the intramolecular distance (in angstroms) between the donor's hydrogen and oxygen, and column C shows the supplement angle of the hydrogen bond.

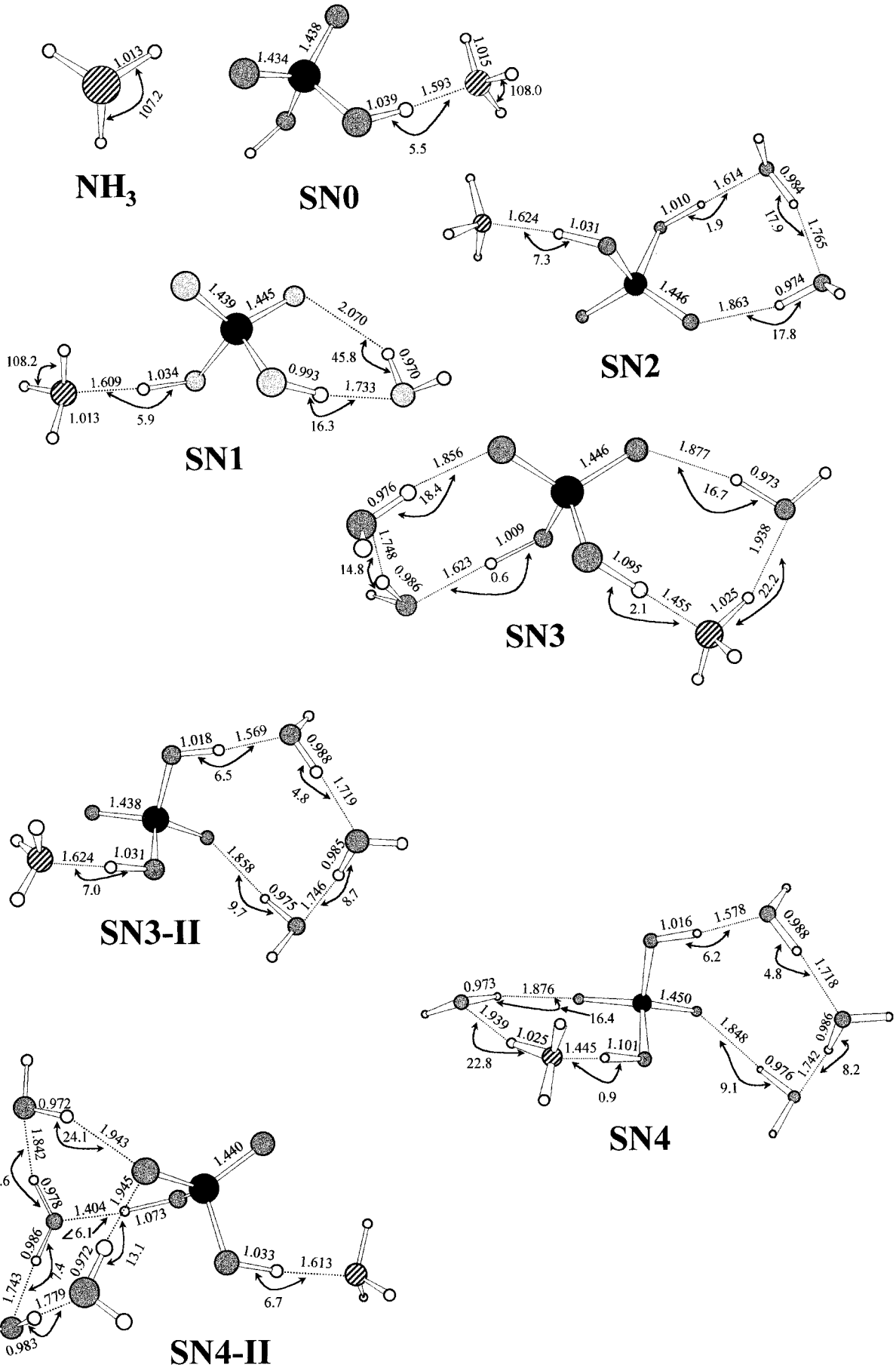

Figure 1. Structures of NH_3 and $NH_3 \cdot H_2SO_4 \cdot nH_2O$ ($n = 0-5$) calculated at B3LYP/6-311++G(2d,2p)//B3LYP/6-311++G(2d,2p). Angles are in degrees and bond lengths are in angstroms. Angles for hydrogen bonds are supplement angles: $180° - \angle O-H\cdots O$.

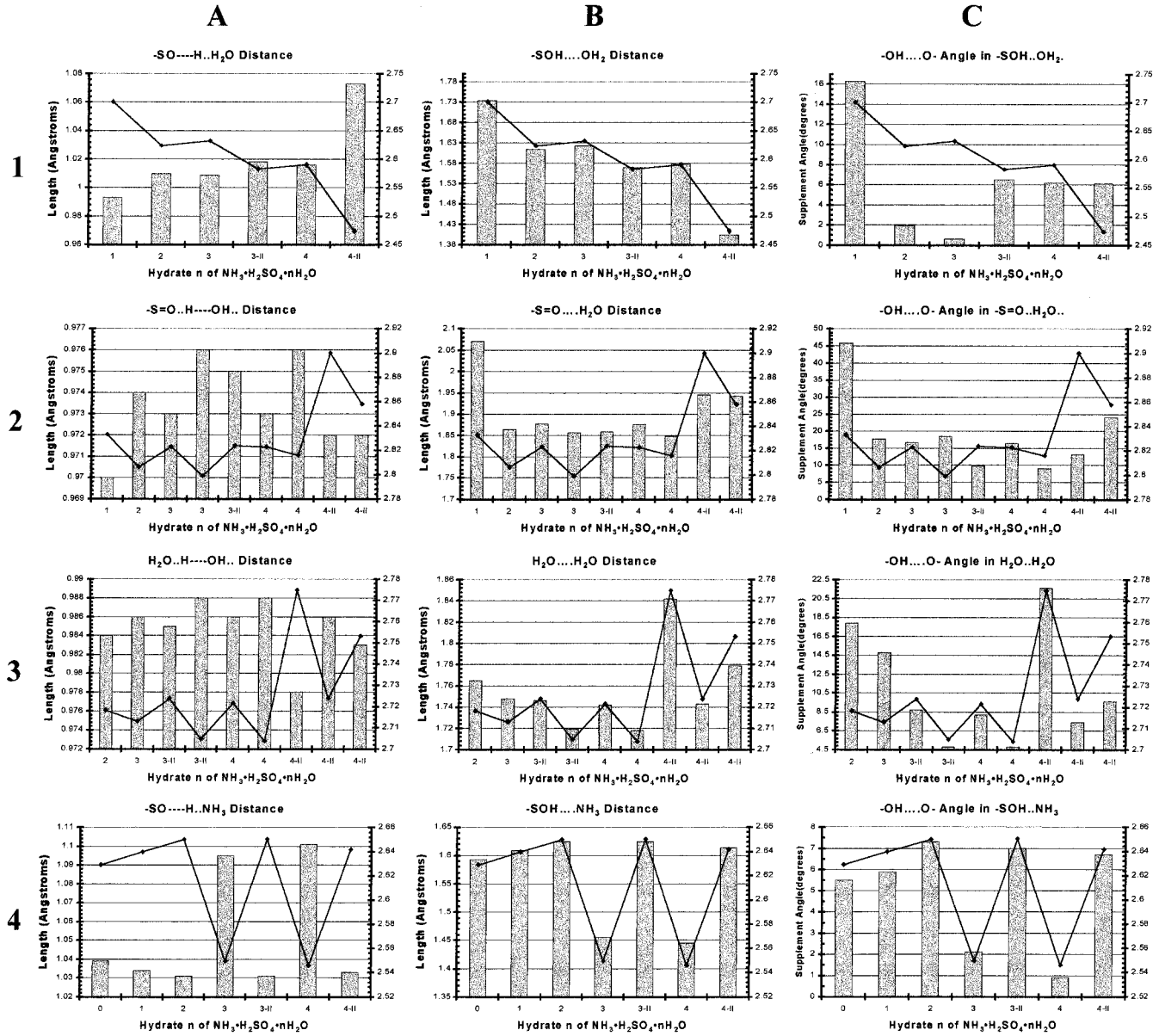

Figure 2. Hydrogen bond descriptor plots for NH_3 and $NH_3 \cdot H_2SO_4 \cdot nH_2O$ ($n = 0-5$). The left *y*-axis on each subplot corresponds to the histograms. The right *y*-axis on each subplot corresponds to the line graph. See text for a full explanation.

Each row of Figure 2 shows the number of different types of hydrogen bonds present in this system. There are five different types of hydrogen bonds in this system:

sulfuric acid −OH to water	(1)
sulfuric acid π-d O to water	(2)
water to water hydrogen bonds	(3)
sulfuric acid to ammonia hydrogen bonds	(4)
water to ammonia hydrogen bonds	(5)

Only the first four are plotted, the fifth type only occurs in SN3 and SN4. Subplots 1−4 have on the right *y*-axis the distance between the two oxygens involved in the hydrogen bonding, *R*(O−O). Subplot 5 has on its right *y*-axis the distance between the oxygen and nitrogen atoms involved in the hydrogen bonding, *R*(N−O). Figure 3 shows the rotational constants and dipole moments for each hydrate.

NH_3. Ammonia is shown in Figure 1. The bond lengths and angle are in excellent agreement (a deviation of 0.001 Å and 0.5°) with experimental results.[29] In addition, the MP2(fc)/6-311++G(d,p) results of Tao[30] are also in agreement with an equilibrium bond length of 1.014 Å and the same bond angle,

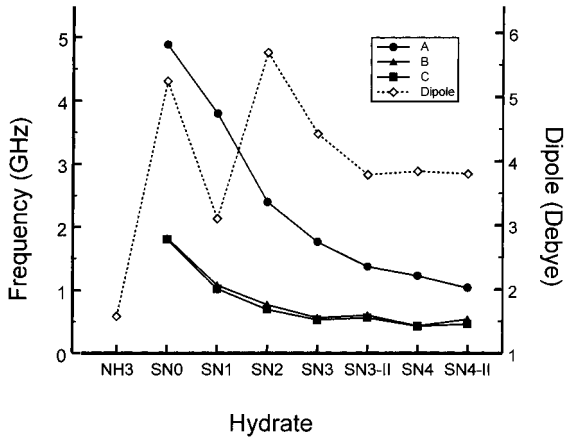

Figure 3. Rotational constants and dipole moments for NH_3 and $NH_3 \cdot H_2SO_4 \cdot nH_2O$ ($n = 0-5$).

but the calculated dipole moment differs with 1.57 D for B3LYP/6-311++G(2d,2p) while the MP2 result is 1.74 D. The experimental dipole value for NH_3 is 1.51 D,[29] which is quite close to the B3LYP's calculated value.

$NH_3 \cdot H_2SO_4$. A very good candidate for a global minimum for SN0 is the one shown in Figure 1. SN0 has a strong type 4 hydrogen bond with HBD of (1.59, 1.04, 5.5). Figure 3 shows that the largest moments (rotational constants C and B) of inertia for $NH_3 \cdot H_2SO_4$ are about the same, indicative of the somewhat oblateness of this molecule. There is a significant increase in the dipole moment. This is primarily due to the alignment of the NH_3's dipole with respect to the bonded −SOH.

$NH_3 \cdot H_2SO_4 \cdot H_2O$. Only one conformer has been located for SN1. This should be the most stable since it involves a strong type 4 and type 1 hydrogen bond. SN1 has the largest R(O−O) distance for its type 1 hydrogen bond, primarily caused by the high ring strain in its hydrogen bonds, as shown in column C of Figure 2. The rotational constants of the SN1 naturally decrease because of the additional water molecule. Rotational constant A experiences a larger decrease due to the water becoming bonded to the −SOH on the other "side" of H_2SO_4. The dipole decreases due to the partial opposing alignment of the added water molecule's dipole on the −SOH.

We tried to locate a neutral in which one water is on the same "side" as the NH_3, but the starting molecule converged into the double ion of SN1D. A possible explanation of this behavior is given below in $NH_3 \cdot H_2SO_4 \cdot 2H_2O$.

$NH_3 \cdot H_2SO_4 \cdot 2H_2O$. One conformer of SN2 has been found. The addition of a water where the NH_3 is located yields the double ion SN2D-II. The R(O−O) distances for the type 1 and type 2 hydrogen bonds decrease, which is primarily attributed to the decrease in ring strain and optimal overlap of the two oxygen and hydrogen atom MO's involved in the hydrogen bond formation. The R(N−O) distance of the type 4 hydrogen bond undergoes a slight increase. Rotational constant A undergoes another fairly large decrease due to the additional water molecule on the other "side" of H_2SO_4 with respect to NH_3. The additional water's dipole is partially aligned with the −SOH's dipole on the same "side", resulting in an increase of the overall dipole moment.

We tried to find a neutral in which one water is on the same "side" as the NH_3 for $NH_3 \cdot H_2SO_4 \cdot 2H_2O$, but the starting neutral structures always formed double ions. One possible explanation is that in the smaller hydrates (SN1, SN2), placing a water next to the NH_3, places this unstable system close to its respective double ion (SN1D and SN2D-II). This unstable system will start to form its double ion. When forming its double ion, the system will stabilize itself by reducing the Coulombic interaction between the forming NH_4^+ and HSO_3^- by both reducing the electron density around the HSO_3^- (removing the electron density from the lone pair on the water on the other "side") and by increasing the distance between the counterions.[32] It appears that the starting neutrals SN1-II and SN2-II appear to carry out this procedure as they only form their respective double ions SN1D and SN2D-II. It is possible to form neutral molecules in $NH_3 \cdot H_2SO_4 \cdot 3H_2O$ (SN3) and $NH_3 \cdot H_2SO_4 \cdot 4H_2O$ (SN4) where a water molecule is next to NH_3. This could be due to the increase of electron density. This increase in electron density is from the multiple lone pairs on the H_2O's on the other side. This increase in electron density on that side inhibits the formation of the double ion, so a minimum forms on the potential energy surface for hydrates of this size and type.

$NH_3 \cdot H_2SO_4 \cdot 3H_2O$. Two conformers haven been found: SN3 and SN3-II. SN3 is more stable than SN3-II (see Hydrate Energetics below). This is primarily due to the increased interaction of H_2SO_4 with the water molecules in SN3 than in SN3-II. As demonstrated in a previous paper,[31] water−water interactions are less exothermic than water−sulfuric acid interactions. There is actually a slight increase of the R(O−O) distances for type 1−3 hydrogen bonds, but there is a tremendous decrease in the R(N−O) distance for the type 4 hydrogen bond. The expected decrease in all three rotational constants continues for these conformers, as shown in Figure 3. Also, there is a decrease in dipole moment in both conformers.

$NH_3 \cdot H_2SO_4 \cdot 4H_2O$. Two conformers have been located for $NH_3 \cdot H_2SO_4 \cdot 4H_2O$: SN4 and SN4-II. SN4 is more stable than SN4-II (see Hydrate Energetics below). Once again this is primarily due to the increased interaction of H_2SO_4 with the water molecules in SN4 than in SN4-II. The type 1 hydrogen bond with a HBD of (1.40, 1.07, 6.1) in SN4-II is the shortest hydrogen bond among all the neutrals and double ions.

The R(O−O) and R(N−O) distances for all four types of hydrogen bonds of SN4 are shown in Figure 2. The additional water causes the expected decrease in all three rotational constants. There is practically no change in the dipole moment for both conformers.

$NH_3 \cdot H_2SO_4 \cdot 5H_2O$. All starting neutral structures for $NH_3 \cdot H_2SO_4 \cdot 5H_2O$ converged into one of the double ions explained in the next part. If there is more than one water molecule present on the same side with NH_3, a double ion forms. It probably is possible to form a neutral with all five water molecules present on one side, but it is very unlikely that such a neutral will be more stable than the corresponding double ion, as explained in the Hydrate Energetics section.

Double Ions. Structures for $NH_4^+ \cdot HSO_4^- \cdot nH_2O$ ($n = 1-5$) are shown in Figure 4. Figure 5 shows a general trend of the HBD's of each neutral. Column A of Figure 5 shows the donor's intermolecular hydrogen bond distance with increasing hydrate size, column B of Figure 5 shows the intramolecular distance (in angstroms) between the donor's hydrogen and oxygen and column C shows the supplement angle of the hydrogen bond. Each row of Figure 5 shows the number of different types of hydrogen bonds present in this system. There are six different types of hydrogen bonds in this system:

sulfuric acid −OH to water	(1)
sulfuric acid π-d O to water	(2)
water to water hydrogen bonds	(3)
water to ammonium hydrogen bonds	(4)
sulfuric acid to ammonium hydrogen bonds	(5)
water to sulfuric acid's O in −SOH	(6)

Each subplot has on its right y-axis the oxygen−oxygen (or nitrogen−oxygen) distance involved in the hydrogen bonding, R(O−O) or R(N−O). Figure 6 shows the rotational constants and dipoles for each hydrate.

NH_4^+. The ammonium ion is shown in Figure 4. The bond lengths are in perfect agreement with the MP2/6-311++G(d,p) results of Tao.[30]

$NH_4^+ \cdot HSO_4^-$. There are no double ions of $NH_4^+ \cdot HSO_4^-$. Any starting double ion of $NH_4^+ \cdot HSO_4^-$ collapsed into its neutral. This is mainly because there are no water molecules to separate the two ions. Without this separation, the electrostatic interaction energy is very large, and consequently, those structures do not exist on the potential energy surface.[32]

$NH_4^+ \cdot HSO_4^- \cdot H_2O$. One conformer has been located for $NH_4^+ \cdot HSO_4^- \cdot H_2O$. Previous studies of double ions have shown

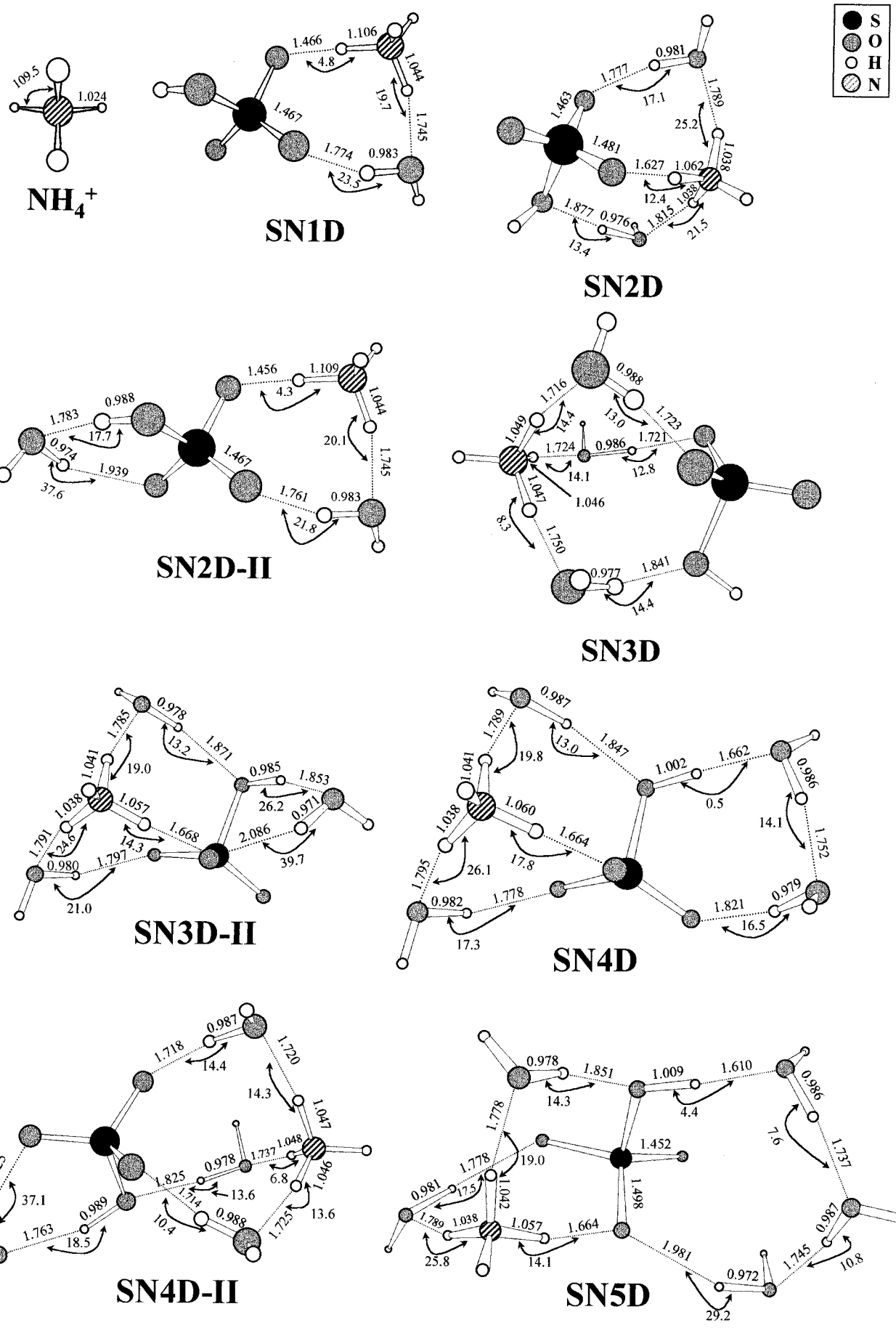
S
O
H
N
109.5
1.024
NH4+
1.466
1.106
4.8
1.044
19.7
1.467
1.745
1.774
0.983
23.5
SN1D
0.981
1.777
17.1
1.789
25.2
1.463
1.481
1.038
1.627
1.062
12.4
1.038
1.877
0.976
1.815
21.5
13.4
SN2D
1.456
1.109
4.3
1.044
20.1
1.783
0.988
17.7
0.974
1.467
1.745
1.939
37.6
1.761
0.983
21.8
SN2D-II
0.988
1.716
1.723
13.0
1.049
14.4
1.724
0.986
1.721
12.8
14.1
1.047
1.046
8.3
1.750
0.977
1.841
14.4
SN3D
0.978
1.785
13.2
1.871
1.041
19.0
0.985
1.853
26.2
1.038
1.057
0.971
1.791
24.6
1.668
2.086
14.3
0.980
1.797
39.7
21.0
SN3D-II
0.987
1.789
19.8
13.0
1.847
1.041
1.002
1.662
0.5
0.986
1.038
1.060
14.1
1.752
1.664
17.8
1.795
26.1
0.982
1.778
1.821
0.979
16.5
17.3
SN4D
0.987
1.718
14.4
1.720
14.3
1.047
1.925
37.1
1.048
0.978
1.737
6.8
1.046
1.825
13.6
0.989
1.714
13.6
0.975
1.763
18.5
10.4
0.988
1.725
SN4D-II
0.978
1.851
1.009
1.610
14.3
4.4
0.986
1.778
7.6
1.737
1.452
19.0
1.778
0.981
1.042
1.498
17.5
1.789
1.038
1.057
1.664
0.987
25.8
14.1
1.981
1.745
10.8
0.972
29.2
SN5D

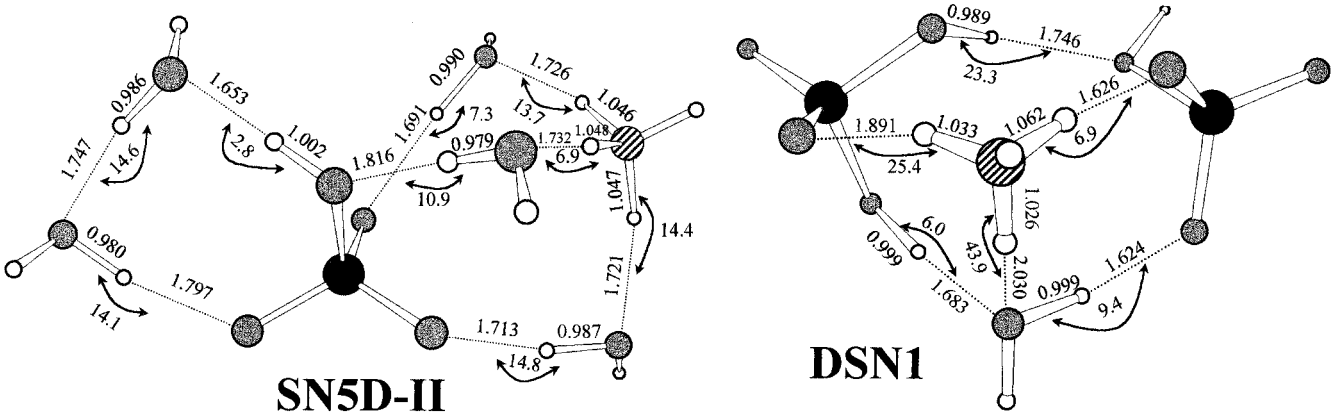

Figure 4. Structures of NH_4^+ and $NH_4^+ \cdot HSO_4^- \cdot nH_2O$ ($n = 1-5$) calculated at B3LYP/6-311++G(2d,2p)//B3LYP/ 6-311++G(2d,2p). Angles are in degrees and bond lengths are in angstroms. Angles for hydrogen bonds are supplement angles: $180° - \angle O-H\cdots O$.

that several water molecules are required to reduce the electrostatic interaction enough to form double ions.[32−35] It seems for SN1D only one molecule of water is sufficient. This at least qualitatively shows that NH_3 has a greater proton affinity than the bases examined in those previous studies. SN1D is not as stable as its corresponding neutral SN1 (see Table 2). The double ions do not become more stable than their corresponding neutral until SN4D. Figure 5 shows that there is a contraction over all the different types of hydrogen bonds with respect to its neutral. This is also shown in the SN1D's rotational constants. The partial separation of charges in SN1D causes its dipole to be much larger than its corresponding neutral SN1.

$NH_4^+ \cdot HSO_4^- \cdot 2H_2O$. Two conformers have been located for $NH_4^+ \cdot HSO_4^- \cdot 2H_2O$: SN2D and SN2D-II. SN2D is more stable than SN2D-II primarily due to the enhanced electrostatic interaction of the NH_4^+ with three electron pairs. In addition, SN2D-II contains (on the "left" side) a strained ring, resulting in large supplementary angles for some of its hydrogen bonds, as shown in column C of Figure 5. Also, Figure 5 also shows the R(N−O) distance is closer between the two ions in SN2D-II, resulting in increased electrostatic interaction between the ions. In fact, SN2D-II has the shortest hydrogen bond R(N−O) distance of the double ions for its type 5 hydrogen bond with a HBD of (1.46, 1.11, 4.3). SN2D has a more spherical shape than SN2D-II, as shown by its rotational constants in Figure 6. SN2D-II also experiences a slight dip in dipole moment due to the somewhat misalignment of the additional water molecule's dipole.

$NH_4^+ \cdot HSO_4^- \cdot 3H_2O$. There are two conformers for $NH_4^+ \cdot HSO_4^- \cdot 3H_2O$: SN3D and SN3D-II. SN3D is a more stable double ion than SN3D-II for reasons very similar to those presented for SN2D and SN2D-II above. Note the diamond-like shape "cap" in SN3D (ignoring hydrogens). Such "caps" have been located in other double ions structure studied in the past,[31−34,36] as they tend to be the most stable shape. SN3D and SN3D-II have similar shapes, as shown by their similar rotational constants, but their dipole moments differ mainly due to the alignment of the three water dipoles in the diamond "cap".

$NH_4^+ \cdot HSO_4^- \cdot 4H_2O$. Two conformers for $NH_4^+ \cdot HSO_4^- \cdot 4H_2O$ were found: SN4D and SN4D-II. The structure containing the diamond-like "cap" now is the less stable. This could be primarily due to ring strain experienced by the lone water on the "right" side of the structure. SN4D and SN4D-II also have similar shapes, as shown by their similar rotational constants, but their dipole moments differ.

$NH_4^+ \cdot HSO_4^- \cdot 5H_2O$. There are also two conformers for $NH_4^+ \cdot HSO_4^- \cdot 5H_2O$: SN5D and SN5D-II. Both structures are about the same stability. SN5D-II contains the familiar diamond shape "cap", while SN5D does not. Both SN5D and SN5D-II contain the smallest R(O−O) and R(N−O) distances for most types of hydrogen bonds (Figure 5). It is noteworthy that by ignoring the unstable conformers of the double ions and examining Figure 5, one can see that there is a general decrease in the R(O−O) distances of types 1, 2, 3, and 6 hydrogen bonds. The conformers have nearly identical rotational constants, indicating similar distributions of nuclear mass. Both conformers' dipole moments are very different. As stated before, this is mainly due to the alignment of the three water dipoles in the diamond "cap".

$NH_4^+ \cdot HSO_4^- \cdot H_2SO_4 \cdot H_2O$. $NH_3 \cdot H_2SO_4 \cdot H_2O \cdot H_2SO_4$ was examined to see if it exists and if it provided additional free energy to allow further growth through addition of $-H_2SO_4 \cdot 2H_2O-$ monomers, as described in our previous paper.[31] $NH_3 \cdot H_2SO_4 \cdot H_2O \cdot H_2SO_4$ actually converged into a double ion, $NH_4^+ \cdot HSO_4^- \cdot H_2O \cdot H_2SO_4$ (DSN1), as shown in Figure 4. $NH_4^+ \cdot HSO_4^- \cdot H_2O \cdot H_2SO_4$ is similar to SN1D except for the additional H_2SO_4 that is hydrogen bonded in three places.

Hydrate Energetics

Shown in Table 2 are the relative enthalpies, entropies, and free energies between hydrates, $NH_3 \cdot H_2SO_4 \cdot nH_2O$, of the same n. Note as the number of waters are increased, the double ion form of $NH_3 \cdot H_2SO_4 \cdot nH_2O$ is energetically more favorable. Our previous study[31] has shown a similar finding with $H_2SO_4 \cdot nH_2O$ except the double ion is not energetically favorable until $n = 7$, where in this study it occurs at $n = 4$ for $NH_3 \cdot H_2SO_4 \cdot nH_2O$. This agrees with the fact that ammonia is a stronger base than water. Also, such neutral to double ion transitions have been observed experimentally for naphthol in water in which the equilibrium shifts toward the protonated naphthol as more waters are added to naphthol.[37]

The electronic energy and the zero-point vibrational energy are given in Table 1 as well as the thermal energy and entropy at 173, 198, 223, 248, 273, and 298 K for each of the hydrates studied. The electronic energies, thermal energies, and entropies for H_2O and $H_2SO_4 \cdot nH_2O$, $n = 0-6$ used in the $NH_3 \cdot H_2SO_4 \cdot nH_2O$ energetics calculations were taken from our previous paper.[31] The temperature range was selected to correspond to the approximate range of temperatures found in the troposphere and stratosphere. Free energies, entropies, enthalpies, and internal energies of formation of the $NH_3 \cdot H_2SO_4 \cdot nH_2O$ from $H_2SO_4 \cdot nH_2O + NH_3$ and $NH_3 \cdot H_2SO_4 \cdot (n-1)H_2O + H_2O$ at 298 K and 1 atm are given in Table 2. Free energies, entropies, and enthalpies of $NH_3 \cdot H_2SO_4 \cdot nH_2O$ from $H_2SO_4 \cdot nH_2O + NH_3$

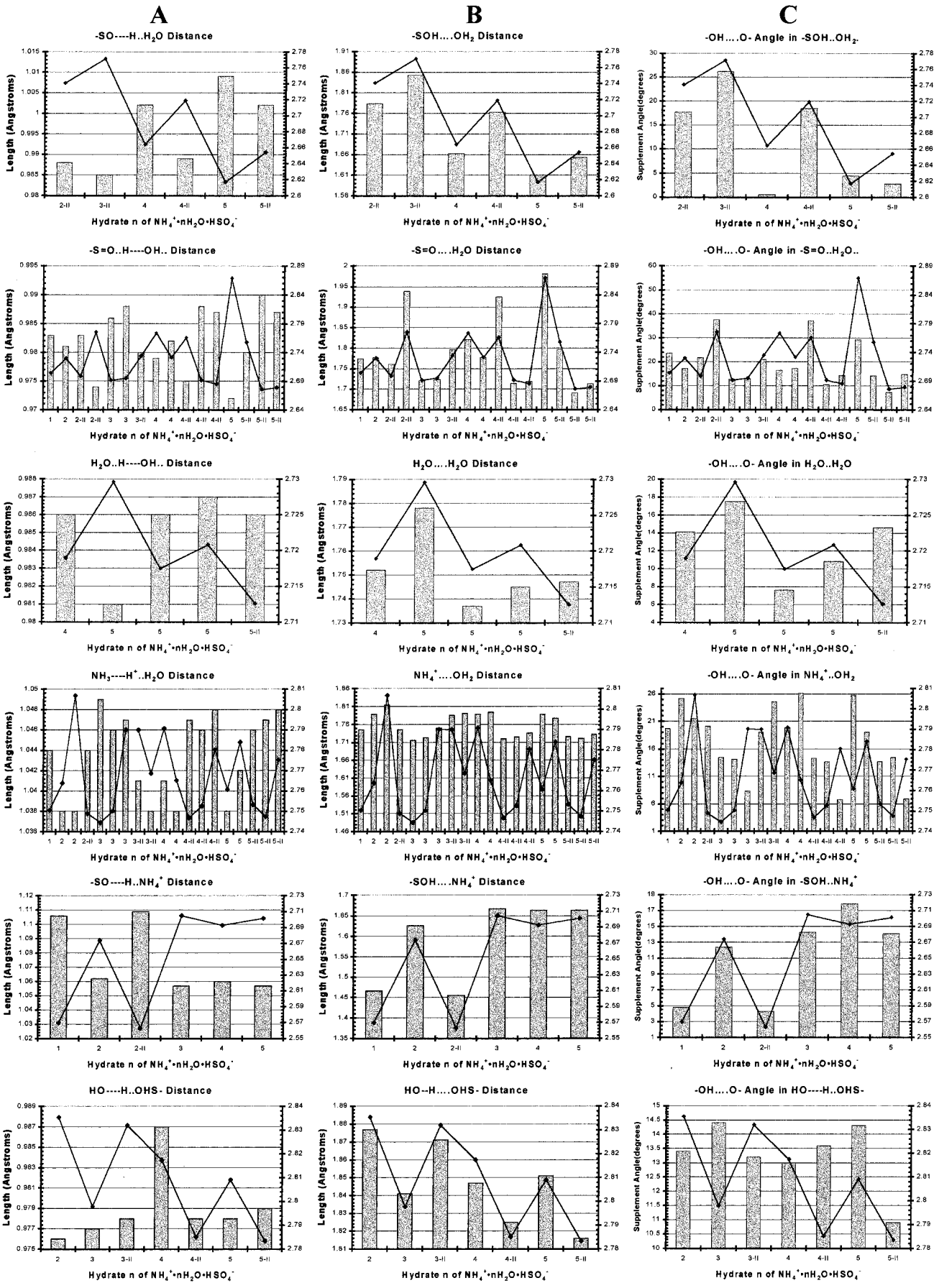

Figure 5. Hydrogen bond descriptor plots for $NH_4^+ \cdot HSO_4^- \cdot nH_2O$ ($n = 1-5$). The left *y*-axis on each subplot corresponds to the histograms. The right *y*-axis on each subplot corresponds to the line graph. See text for a full explanation.

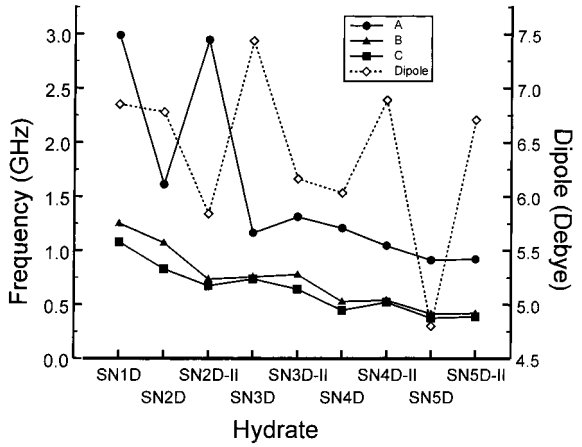

Figure 6. Rotational constants and dipole moments for $NH_4^+ \cdot HSO_4^- \cdot nH_2O$ ($n = 1-5$).

TABLE 2: Enthalpy (kcal/mol), Entropy [cal/(mol K)], and Gibbs Free Energy (kcal/mol) of Isomerization for the Hydrates of Sulfuric Acid at 298 K and 1 atm

	ΔH	ΔS	ΔG
Neutral to Neutral Isomerizations			
$NH_3 \cdot H_2SO_4 \cdot 3H_2O \leftrightarrow$ NH3·$H_2SO_4 \cdot 3H_2O$-II	1.44	1.45	1.01
$NH_3 \cdot H_2SO_4 \cdot 4H_2O \leftrightarrow$ NH3·$H_2SO_4 \cdot 4H_2O$-II	0.22	−2.77	1.05
Double Ion to Double Ion Isomerization			
$NH_4^+ \cdot HSO_4^- \cdot 2H_2O \leftrightarrow NH_4^+ \cdot HSO_4^- \cdot 2H_2O$-II	2.11	2.31	1.42
$NH_4^+ \cdot HSO_4^- \cdot 3H_2O \leftrightarrow NH_4^+ \cdot HSO_4^- \cdot 3H_2O$-II	−0.05	−2.19	0.60
$NH_4^+ \cdot HSO_4^- \cdot 4H_2O \leftrightarrow NH_4^+ \cdot HSO_4^- \cdot 4H_2O$-II	2.10	3.11	1.18
$NH_4^+ \cdot HSO_4^- \cdot 5H_2O \leftrightarrow NH_4^+ \cdot HSO_4^- \cdot 5H_2O$-II	−0.16	−0.68	0.05
Double Ionic to Neutrals Isomerization			
$NH_4^+ \cdot HSO_4^- \cdot H_2O \leftrightarrow$ NH3·$H_2SO_4 \cdot H_2O$	0.04	2.37	−0.67
$NH_4^+ \cdot HSO_4^- \cdot 2H_2O \leftrightarrow$ NH3·$H_2SO_4 \cdot 2H_2O$	1.76	6.04	−0.04
$NH_4^+ \cdot HSO_4^- \cdot 3H_2O \leftrightarrow$ NH3·$H_2SO_4 \cdot 3H_2O$	−0.02	4.14	−1.26
$NH_4^+ \cdot HSO_4^- \cdot 4H_2O \leftrightarrow$ NH3·$H_2SO_4 \cdot 4H_2O$	3.93	7.62	1.65

over the temperatures of 173, 198, 223, 248, and 273 K are given in Table 3. Also, free energies, entropies, and enthalpies of formation of $NH_3 \cdot H_2SO_4 \cdot (n-1)H_2O + H_2O$ over the temperatures of 173, 198, 223, 248, 273, and 298 K are given in Table 4.

Plots of the free energy for the reactions $H_2SO_4 \cdot nH_2O + NH_3 \leftrightarrow NH_3 \cdot H_2SO_4 \cdot nH_2O$ as a function of n are shown in Figure 7. From inspection of Figure 7 it can be seen that all reactions at all temperatures are spontaneous, but the difference in ΔG is positive up to $n = 3$ and negative afterward. The "bump" at $n = 3$ is mainly due to the weaker hydrogen bonding between the additional water and NH_3 leading to a slightly less exothermic reaction. The decrease in ΔG at and after $n = 4$ is due to the formation of the double ion through addition of H_2O. As the temperature is lowered, the $T\Delta S$ term becomes more positive by about 1 kcal/mol per 25 °C, resulting in lowering of ΔG by about 1 kcal/mol per 25 °C.

The cumulative free energy of formation of $NH_3 \cdot H_2SO_4 \cdot nH_2O$ from $H_2SO_4 \cdot nH_2O$ and NH_3 is shown in Figure 7 for each of the hydrates studied. Figure 7 shows that all the higher hydrates of $NH_3 \cdot H_2SO_4 \cdot nH_2O$ approximately linearly decrease in free energy of the system for hydrates 0−5.

Plots of the free energy for the reactions $NH_3 \cdot H_2SO_4 \cdot (n-1)H_2O + H_2O \leftrightarrow NH_3 \cdot H_2SO_4 \cdot nH_2O$ as a function of n are shown in Figure 8. The magnitude of the free energies of the reaction $NH_3 \cdot H_2SO_4 \cdot (n-1)H_2O + H_2O \leftrightarrow NH_3 \cdot H_2SO_4 \cdot nH_2O$ are less than those of $H_2SO_4 \cdot nH_2O + NH_3 \leftrightarrow NH_3 \cdot H_2SO_4 \cdot nH_2O$ mainly because the addition of NH_3 is a much more exothermic reaction since NH_3 is a stronger base than water. For 25 °C all the ΔG's are around 0 kcal/mol. As the temperature is lowered, the $T\Delta S$ term becomes more positive by about 0.75 kcal/mol per 25 °C, resulting in a lowering of ΔG by about 0.75 kcal/mol per 25 °C. A similar trend was shown in a previous study[8] on $(H_2SO_4)_2 \cdot (n-1)H_2O + H_2O \leftrightarrow (H_2SO_4)_2 \cdot nH_2O$, $n = 1-6$.

The cumulative free energy of formation of $NH_3 \cdot H_2SO_4 \cdot nH_2O$ from $NH_3 \cdot H_2SO_4 \cdot (n-1)H_2O$ and H_2O is shown in Figure 8 for each of the hydrates studied. There is a slight thermodynamic free energy barrier at temperatures of 0 °C and above, which could hinder higher hydrate formation.

Atmospheric Implications. By examining the free energies for the formation of $(H_2SO_4)_2 \cdot nH_2O$ from $H_2SO_4 \cdot nH_2O + H_2SO_4$, $n = 0-6$,[8] one can see that they are all about equal to or greater in free energy than the reactions producing $NH_4^+ \cdot HSO_4^- \cdot H_2O \cdot H_2SO_4$. This is most unfortunate. A thermodynamic and kinetic analysis was invoked in our previous paper to examine the possible formation of $(H_2SO_4)_2 \cdot nH_2O$. Both analyses showed that $(H_2SO_4)_2 \cdot nH_2O$ cannot form without some "help". A similar conclusion can be brought about here since the free energies for the formation of $NH_4^+ \cdot HSO_4^- \cdot H_2O \cdot H_2SO_4$ from $H_2SO_4 \cdot H_2O + NH_3 \cdot H_2SO_4$ and $H_2SO_4 + NH_3 \cdot H_2SO_4 \cdot H_2O$ are similar to those in our previous paper. This can lead to more questions as to the importance NH_3 has in the formation of atmospheric particles. NH_3 does have an important role in the atmosphere. Its role is to increase the pH of atmospheric particles. The calculated free energies show that NH_3 appears to not have any role in the nucleation of new atmospheric particles despite the

TABLE 3: Thermodynamic DFT Results at 298 K and 1 atm[a]

	ΔE	ΔH	ΔS	ΔG	K_p
Addition by NH_3					
$NH_3 + H_2SO_4 \leftrightarrow NH_3 \cdot H_2SO_4$	−13.17	−13.76	−30.91	−4.54	2117.90
$NH_3 + H_2SO_4 \cdot H_2O \leftrightarrow NH_3 \cdot H_2SO_4 \cdot H_2O$	−12.32	−12.91	−31.09	−3.64	463.47
$NH_3 + H_2SO_4 \cdot 2H_2O \leftrightarrow NH_3 \cdot H_2SO_4 \cdot 2H_2O$	−12.05	−12.64	−30.56	−3.53	385.83
$NH_3 + H_2SO_4 \cdot 3H_2O \leftrightarrow NH_3 \cdot H_2SO_4 \cdot 3H_2O$	−11.65	−12.24	−31.74	−2.77	107.47
$NH_3 + H_2SO_4 \cdot 4H_2O \leftrightarrow NH_4^+ \cdot HSO_4^- \cdot 4H_2O$	−13.61	−14.20	−36.79	−3.23	232.56
$NH_3 + H_2SO_4 \cdot 5H_2O \leftrightarrow NH_4^+ \cdot HSO_4^- \cdot 5H_2O$	−15.15	−15.74	−36.73	−4.79	3197.97
Addition by H_2O					
$NH_3 \cdot H_2SO_4 + H_2O \leftrightarrow NH_3 \cdot H_2SO_4 \cdot H_2O$	−8.28	−8.87	−30.70	0.29	0.62
$NH_3 \cdot H_2SO_4 \cdot H_2O + H_2O \leftrightarrow NH_3 \cdot H_2SO_4 \cdot 2H_2O$	−8.41	−9.00	−30.12	−0.02	1.04
$NH_3 \cdot H_2SO_4 \cdot 2H_2O + H_2O \leftrightarrow NH_3 \cdot H_2SO_4 \cdot 3H_2O$	−8.86	−9.45	−32.47	0.23	0.67
$NH_3 \cdot H_2SO_4 \cdot 3H_2O + H_2O \leftrightarrow NH_4^+ \cdot HSO_4^- \cdot 4H_2O$	−10.74	−11.33	−37.65	−0.10	1.19
$NH_4^+ \cdot HSO_4^- \cdot 4H_2O + H_2O \leftrightarrow NH_4^+ \cdot HSO_4^- \cdot 5H_2O$	−10.93	−11.52	−37.18	−0.43	2.08
Special					
$H_2SO_4 \cdot H_2O + NH_3 \cdot H_2SO_4 \leftrightarrow NH_4^+ \cdot H_2O \cdot H_2SO_4 \cdot HSO_4^-$	−15.19	−15.78	−48.03	−1.46	11.74
$H_2SO_4 + NH_3 \cdot H_2SO_4 \cdot 3H_2O \leftrightarrow NH_4^+ \cdot H_2O \cdot H_2SO_4 \cdot HSO_4^-$	−16.04	−16.63	−47.85	−2.36	53.63

[a] ΔE, ΔH, and ΔG are in kcal/mol, ΔS is in cal/(mol K).

TABLE 4: ΔH and ΔG (kcal/mol) and ΔS [cal/(mol K)] for the Reactions of $H_2SO_4 \cdot nH_2O + NH_3 \leftrightarrow NH_3 \cdot H_2SO_4 \cdot nH_2O$ ($n = 0-5$) at the Temperatures Indicated

	273 K				248 K				223 K				198 K				173 K			
	ΔH	ΔS	ΔG	K_p	ΔH	ΔS	ΔG	K_p	ΔH	ΔS	ΔG	K_p	ΔH	ΔS	ΔG	K_p	ΔH	ΔS	ΔG	K_p
$NH_3 \cdot H_2SO_4$	−13.8	−31.0	−5.3	17721	−13.8	−31.0	−6.1	228494	−13.8	−31.1	−6.9	5.2×10^6	−13.8	−31.1	−7.6	2.7×10^8	−13.8	−31.1	−8.4	4.2×10^{10}
$NH_3 \cdot H_2SO_4 \cdot H_2O$	−12.9	−31.1	−4.4	3403	−12.9	−31.2	−5.2	37519	−12.9	−31.2	−6.0	7.1×10^5	−12.9	−31.2	−6.8	2.8×10^7	−12.9	−31.1	−7.5	3.2×10^9
$NH_3 \cdot H_2SO_4 \cdot 2H_2O$	−12.7	−30.6	−4.3	2720	−12.7	−30.6	−5.1	28442	−12.7	−30.6	−5.8	5.0×10^5	−12.6	−30.6	−6.6	1.8×10^7	−12.6	−30.5	−7.4	1.9×10^9
$NH_3 \cdot H_2SO_4 \cdot 3H_2O$	−12.3	−31.8	−3.6	711	−12.3	−31.9	−4.4	6926	−12.3	−31.9	−5.2	1.1×10^5	−12.3	−32.0	−6.0	3.7×10^6	−12.3	−31.9	−6.8	3.4×10^8
$NH_4^+ \cdot HSO_4^- \cdot 4H_2O$	−14.2	−36.9	−4.2	2082	−14.2	−36.9	−5.1	29211	−14.2	−36.9	−6.0	7.4×10^5	−14.2	−36.9	−6.9	4.2×10^7	−14.2	−36.7	−7.8	7.7×10^9
$NH_4^+ \cdot HSO_4^- \cdot 5H_2O$	−15.7	−36.8	−5.7	36274	−15.8	−36.8	−6.6	675428	−15.8	−36.8	−7.5	2.4×10^7	−15.7	−36.8	−8.5	2.1×10^9	−15.7	−36.6	−9.4	6.8×10^{11}

TABLE 5: ΔH and ΔG (kcal/mol) and ΔS [cal/(mol K)] for the Reactions of $NH_3 \cdot H_2SO_4 \cdot (n-1)H_2O + H_2O \leftrightarrow NH_3 \cdot H_2SO_4 \cdot nH_2O$ ($n = 1-5$) at the Temperatures Indicated

	273 K				248 K				223 K				198 K				173 K			
	ΔH	ΔS	ΔG	K_p	ΔH	ΔS	ΔG	K_p	ΔH	ΔS	ΔG	K_p	ΔH	ΔS	ΔG	K_p	ΔH	ΔS	ΔG	K_p
$NH_3 \cdot H_2SO_4 \cdot H_2O$	−8.9	−30.8	−0.5	2	−8.9	−30.8	−1.3	13	−8.9	−30.8	−2.0	95	−8.9	−30.8	−2.8	1190	−8.9	−30.6	−3.6	3.1×10^4
$NH_3 \cdot H_2SO_4 \cdot 2H_2O$	−9.0	−30.2	−0.8	4	−9.0	−30.2	−1.5	22	−9.0	−30.2	−2.3	172	−9.0	−30.1	−3.0	2225	−9.0	−30.0	−3.8	6.0×10^4
$NH_3 \cdot H_2SO_4 \cdot 3H_2O$	−9.5	−32.5	−0.6	3	−9.5	−32.6	−1.4	17	−9.5	−32.6	−2.2	145	−9.5	−32.6	−3.0	2142	−9.5	−32.4	−3.8	6.9×10^4
$NH_4^+ \cdot HSO_4^- \cdot 4H_2O$	−11.3	−37.6	−1.0	7	−11.3	−37.6	−2.0	56	−11.3	−37.4	−2.9	718	−11.2	−37.2	−3.9	17633	−11.2	−36.9	−4.8	1.1×10^6
$NH_4^+ \cdot HSO_4^- \cdot 5H_2O$	−11.5	−37.2	−1.4	12	−11.5	−37.1	−2.3	104	−11.5	−37.0	−3.2	1405	−11.4	−36.8	−4.1	36473	−11.4	−36.5	−5.1	2.4×10^6

Figure 7. Successive free energy plot (filled symbols, left axis) and cumulative free energy plot (open symbols, right axis) of the reactions of $H_2SO_4 \cdot nH_2O + NH_3 \leftrightarrow NH_3 \cdot H_2SO_4 \cdot nH_2O$, $n = 0-5$. Reactions that involve hydrates of $n \geq 4$ are actually double ions ($NH_4^+ \cdot HSO_4^- \cdot nH_2O$).

Figure 8. Successive free energy plot (filled symbols, left axis) and cumulative free energy plot (open symbols, right axis) of the reactions of $NH_3 \cdot H_2SO_4 \cdot (n-1)H_2O + H_2O \leftrightarrow NH_3 \cdot H_2SO_4 \cdot nH_2O$, $n = 0-5$. Reactions that involve hydrates of $n \geq 4$ are actually double ions ($NH_4^+ \cdot HSO_4^- \cdot nH_2O$).

considerable interest in this species for its possible role in new atmospheric particle formation.[9-11]

There are four other possibilities that might occur to start the aerosol growth process. One possibility is that there is a third (or more) species present that "helps" the system stabilize clusters of $(H_2SO_4)_2 \cdot 2H_2O$ and/or increase the concentration of $X \cdot H_2SO_4 \cdot nH_2O$ ($n = 2, 4, 6$) where X is some stabilizing species. It was mentioned in our previous paper that NH_3 is of prime interest for X, and it is demonstrated in this study that it does not stabilize the system enough. Is there another candidate species for X? There are not enough studies to solidly answer this question, but X must be large enough to reduce the entropy affect that hinders the growth mechanism[8] and X must be able to hydrogen bond to water and sulfuric acid. Candidates for X could be gaseous organics/proteins emitted by biogenic pathways. The organic must have a hydroxyl or carboxylic acid end that can "hook" onto a monomer of $H_2SO_4 \cdot 2H_2O$ or $NH_3 \cdot H_2SO_4 \cdot 2H_2O$. A second possibility is that the free energies calculated are too positive. These clusters are held together by intermolecular hydrogen bonds that are that to be anharmonic[38] there could be some error in the calculated entropies, but recent calculations by Sodupe et al.[23] have shown that B3LYP with very large basis sets can reproduce experimental anharmonic low frequencies of hydrogen-bonded compounds. Also, Scott

and Radom[39] have shown that harmonic frequencies calculated with the B3LYP method compare well with the experimental frequencies of compounds composed of primarily covalent bonds. A third reason is that the reactions initiating the particle growth could form excited-state products, as mentioned in previous papers.[8,40] A fourth and final reason is that there are particles formed from mechanistic fragmentation of macroscopic particles that remain undetected because of their very small size (<2.7 nm, diameter). The current state-of-the-art particle measuring system can only measure particles in the 3 nm diameter range using an Ultrafine Condensation Particle Counter (TSI Inc., St. Paul Minn.). The $-(H_2SO_4)_2 \cdot 2H_2O-$ chain would simply grow on the various exposed sites of these ultrafine particles.

Conclusion

The structures, energetics, dipoles and rotational constants of $NH_3 \cdot H_2SO_4 \cdot nH_2O$ ($n = 0-5$) have been reported. The most stable structures of $NH_3 \cdot H_2SO_4 \cdot nH_2O$, $n = 0-3$, are not double ions and are primarily held together by hydrogen bonds. The structures of $NH_3 \cdot H_2SO_4 \cdot nH_2O$ ($n = 4, 5$) are double ions, producing $NH_4^+ \cdot HSO_4^- \cdot nH_2O$, which are primarily held together by hydrogen bonds and Coulombic electrostatic interaction. All structures of $NH_3 \cdot H_2SO_4 \cdot nH_2O$, $n = 0-5$, can spontaneously form. The molecule $NH_3 \cdot H_2SO_4 \cdot H_2O \cdot H_2SO_4$ was studied to see if it provided enough free energy to initialize the chain growth mechanism of atmospheric particles described by our previous paper.[8] The molecule actually forms a double ion, $NH_4^+ \cdot HSO_4^- \cdot H_2O \cdot H_2SO_4$, and clearly does not have enough free energy to initialize new atmospheric particle growth. This demonstrates that NH_3 could possibly have no role in new atmospheric particle nucleation. It is still unknown as to what species or process initializes new atmospheric particle growth.

Acknowledgment. Support from the Biological/Chemical Oceanography Program, Ocean, Atmosphere and Space Department of the Office of Naval Research (award #N00014-92-J-1281).

References and Notes

(1) Coakley, J. A. J.; Cess, R. D.; Yurevich, F. B. *J. Atmos. Sci.* **1983**, *40*, 116−138.

(2) Charlson, R. J.; Langner, J.; Andreae, M. O.; Warren, S. G. *Tellus* **1991**, *43*, 152−163.

(3) Twomey, S. A.; Piepgrass, M.; Wolfe, T. L. *Tellus* **1984**, *36*, 356−366.

(4) Fouquart, Y.; Isaka, H. *Ann. Geophys.* **1992**, *10*, 462−471.

(5) Farman, J. C.; Murgatroyd, R. J.; Silnickas, A. M.; Thrush, B. A. *Meteorol. Soc.* **1985**, *111*, 1013−1025.

(6) Molina, M. J.; Rowland, F. S. *Nature (London)* **1974**, *249*, 810−812.

(7) Solomon, S. *Rev. Geophys.* **1988**, *26*, 131−148.

(8) Ianni, J. C.; Bandy, A. R. *THEOCHEM*, in review.

(9) Weber, R. J.; Marti, J. J.; McMurry, P. H.; Eisele, F. L.; Tanner, D. J.; Jefferson, A. *J Geophys. Res. Atmos.* **1997**, *102*, 4375−4385.

(10) Weber, R. J.; McMurry, P. H.; Eisele, F. L.; Tanner, D. J. *J. Atmos. Sci.* **1995**, *52*, 2242−2257.

(11) Weber, R. J.; McMurry, P. H.; Mauldin, L.; Tanner, D. J.; Eisele, F. L.; Brechtel, F. J.; Kreidenweis, S. M.; Kok, G. L.; Schillawski, R. D.; Baumgardner, D. *J. Geo. Res.*, in press.

(12) Friend, J. P.; Feeley, H. W.; Krey, P. W.; Spar, J.; Walton, A. *The high altitude sampling program. Vol 5. Supplementary HASP Studies*; Defense Atomic Support Agency: Washington, DC, 1961.

(13) Farlow, N. H.; Snetsinger, K. G.; Hayes, D. M.; Lem, H. Y.; Tooper, B. M. *J. Geophys. Res.* **1978**, *83*, 6207−6211.

(14) Cunningham, W. C.; Etz, E. S.; Zoller, W. H. *Raman microprobe characterization of South Pole aerosol*; San Fransico Press: San Francisco, 1979.

(15) Hayes, D. M.; Ferry, G. V.; Oberbeck, V. R.; Farlow, N. H. Reactivity of stratospheric aerosols in laboratory environments. AGU Spring Mtg, May 22−27, 1980, Toronto, Canada.

(16) Ayers, G. P.; Ivey, J. P. *Tellus* **1986**, *40*, 297−307.

(17) Carslaw, K. S.; Peter, T.; Clegg, S. L. *Rev. Geophys.* **1997**, *35*, 125−154.

(18) Weber, R. J.; McMurry, P., H.; Marti, J. J. *Chem. Eng. Commun.* **1995**, PTL Publication No. 917.

(19) Jaecker-Voirol, A.; Mirabel, P. *Atmos. Environ.* **1989**, *23*, 2053.

(20) Nolan, P. M. Condensation Nuclei Formation by Photooxidation of Sulfur Dioxide with OH Radical in the Presence of Water Vapor and Ammonia, Thesis, Drexel University, 1987.

(21) Becke, A. D. *J. Chem. Phys.* **1993**, *98*, 5648.

(22) Frisch, M. J.; Trucks, G. W.; Schlegel, H. B.; Gill, P. M. W.; Johnson, B. G.; Robb, M. A.; Cheeseman, J. R.; Keith, T.; Petersson, G. A.; Montgomery, J. A.; Raghavachari, K.; Al-Laham, M. A.; Zakrzewsk, V. G.; Ortiz, J. V.; Foresman, J. B.; Cioslowski, J.; Stefanov, B. B.; Nanayakkara, A.; Challacombe, M.; Peng, C. Y.; Ayala, P. Y.; Chen, W.; Wong, M. W.; Andres, J. L.; Replogle, E. S.; Gomperts, R.; Martin, R. L.; Fox, D. J.; Binkley, J. S.; Defrees, D. J.; Baker, J.; Stewart, J. P.; Head-Gordon, M.; Gonzalez, C.; Pople, J. A. *Gaussian 94*, Revision E.2; Gaussian, Inc.: Pittsburgh, PA, 1995.

(23) Sodupe, M.; Oliva, A.; Bertran, J. *J. Phys. Chem.* **1997**, *101*, 9142.

(24) Lundell, J.; Latajka, Z. *J. Phys. Chem.* **1997**, *101*, 5004−5008.

(25) Gonzalez, L.; Mo, O.; Yanez, M. *J. Comput. Chem.* **1997**, *18*, 1124.

(26) Soliva, R.; Orozco, M.; Luque, F. J. *J. Comput. Chem.* **1997**, *18*, 980.

(27) Novoa, J. J.; Sosa, C. *J. Phys. Chem.* **1995**, *99*, 15837.

(28) Bauschlicher, C. W., Jr. *Chem. Phys. Lett.* **1995**, *246*, 40.

(29) Huber, K. P.; Herzberg, G. *Molecular Spectra and Molecular Structure, V. Constants of Polyatomic Molecules*; van Nostrand Reinhold: New York, 1979.

(30) Tao, F.-M. *J. Chem. Phys.* **1998**, *108*, 193−202.

(31) Bandy, A. R.; Ianni, J. C. *J. Phys. Chem. A* **1998**, *102*, 6533−6539.

(32) Planas, M.; Lee, C.; Novoa, J. J. *J. Phys. Chem.* **1996**, *100*, 16495.

(33) Lee, C.; Sosa, C.; Novoa, J. J. *J. Chem. Phys.* **1995**, *103*, 4360.

(34) Lee, C.; Sosa, C.; Planas, M.; Novoa, J. J. *J. Chem. Phys.* **1996**, *104*, 7081.

(35) Kim, K. S.; Dupuis, M.; Lie, G. C.; Clementi, E. *Chem. Phys. Lett.* **1986**, *131*, 451.

(36) Lee, C.; Fitzgerald, G.; Planas, M.; Novoa, J. J. *J. Phys. Chem.* **1996**, *100*, 7398.

(37) Kim, S. K.; Breen, J. J.; Willberg, D. M.; Peng, L. W.; Heikal, A.; Syage, J. A.; Zewail, A. H. *J. Phys. Chem.* **1995**, *99*, 7421.

(38) Rovira, M. C.; Novoa, J. J.; Whangbo, M. H.; Williams, J. M. *Chem. Phys.* **1995**, *200*, 319.

(39) Scott, A. P.; Radom, L. *J. Phys. Chem.* **1996**, *100*, 16502.

(40) Jayne, J. T.; Poschl, U.; Chen, Y.-m.; David, D.; Molina, L. T.; Worsnop, D. R.; Kolb, C. E.; Molina, M. J. *J. Phys. Chem. A.* **1997**, *101*, 10000−10011.